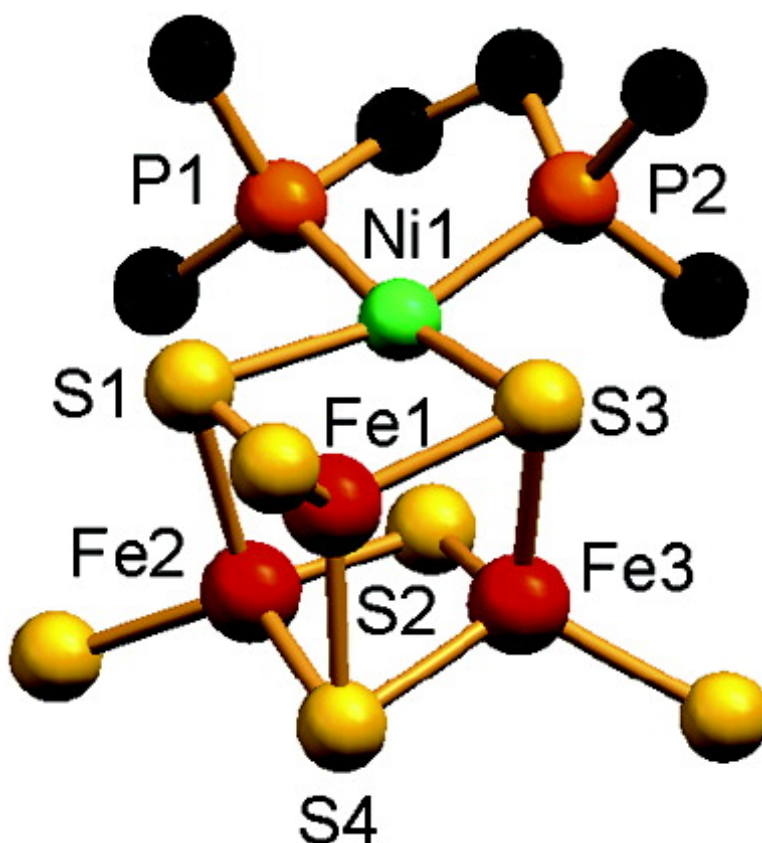


Initial Structure Modification of Tetrahedral to Planar Nickel(II) in a Nickel–Iron–Sulfur Cluster Related to the C-Cluster of Carbon Monoxide Dehydrogenase

Rashmishree Panda, Yugen Zhang, Craig C. McLauchlan, P. Venkateswara Rao, F. A. Tiago de Oliveira, E. Mnck, and R. H. Holm

J. Am. Chem. Soc., **2004**, 126 (20), 6448-6459 • DOI: 10.1021/ja030627s • Publication Date (Web): 29 April 2004

Downloaded from <http://pubs.acs.org> on March 31, 2009



More About This Article

Additional resources and features associated with this article are available within the HTML version:



ACS Publications
 High quality. High impact.

- Supporting Information
- Links to the 1 articles that cite this article, as of the time of this article download
- Access to high resolution figures
- Links to articles and content related to this article
- Copyright permission to reproduce figures and/or text from this article

[View the Full Text HTML](#)



Initial Structure Modification of Tetrahedral to Planar Nickel(II) in a Nickel–Iron–Sulfur Cluster Related to the C-Cluster of Carbon Monoxide Dehydrogenase

Rashmishree Panda,[†] Yugen Zhang,[†] Craig C. McLauchlan,[†]
P. Venkateswara Rao,[†] F. A. Tiago de Oliveira,[‡] E. Münck,^{*,‡} and R. H. Holm^{*,†}

Contribution from the Department of Chemistry and Chemical Biology, Harvard University, Cambridge, Massachusetts 02138, and Department of Chemistry, Carnegie Mellon University, Pittsburgh, Pennsylvania 15213

Received November 17, 2003; E-mail: holm@chemistry.harvard.edu

Abstract: A method has been devised that creates a planar Ni^{II} site from a tetrahedral site in a NiFe₃S₄ cubane-type cluster. Reaction of [(Ph₃P)NiFe₃S₄(LS₃)]²⁻ (**2**) with 1,2-bis(dimethylphosphino)ethane affords [(dmpe)NiFe₃S₄(LS₃)]²⁻ (**3**), isolated in ca. 45% yield as (Et₄N)₂[**3a**]·2.5MeCN and (Et₄N)₂[**3b**]·0.25MeCN, both of which occur in triclinic space group *P* $\bar{1}$. Each crystalline form contains two crystallographically inequivalent clusters with the same overall structure but slightly different dimensions. The cluster is bound by three thiolate terminal ligands to semirigid cavitated ligand LS₃. The NiFe₃S₄ core contains three tetrahedral sites, one Fe(μ_3 -S)₃(SR) and two Fe(μ_3 -S)₂(μ_2 -S)(SR) with normal metric features, and one distorted square planar Ni(μ_3 -S)₂P₂ site in a Ni(μ_3 -S)₂Fe face with mean bond lengths Ni–P = 2.147(9) Å and Ni–S = 2.29(2) Å. The opposite Fe₂(μ_3 -S)(μ_2 -S) face places the μ_2 -S atom at nonbonding and variable distances (2.60–2.90 Å) above the nickel atom. Binding of the strong-field ligand dmpe results in a planar Ni^{II} site and deconstruction of the full cubane geometry. The structure approximates that established crystallographically in the C-cluster of *C. hydrogenoformans* carbon monoxide dehydrogenase whose NiFe₄S₄ core contains a planar NiS₄ site and three tetrahedral FeS₄ sites in a fragment that is bridged by sulfide atoms to an exo iron atom. Mössbauer studies of polycrystalline samples containing both clusters **3a** and **3b** reveal the presence of at least two cluster types. The spectroscopically best defined cluster accounts for ca. 54% of total iron and exhibits hyperfine interactions quite similar to those reported for the *S* = 5/2 state of the protein-bound cubane-type cluster [ZnFe₃S₄]¹⁺, whose Mössbauer spectrum revealed the presence of a high-spin Fe²⁺ site and a delocalized Fe^{2.5+}Fe^{2.5+} pair. Development of reactions leading to a planar nickel and a sulfide-bridged iron atom is requisite to attainment of a synthetic analogue of this complex protein-bound cluster. This work demonstrates a tetrahedral (**2**) → planar (**3**) Ni^{II} stereochemical conversion can be effected by binding of ligands that generate a sufficiently strong in-plane ligand field (dmpe = 1,2-bis(dimethylphosphino)ethane, LS₃ = 1,3,5-tris((4,6-dimethyl-3-mercaptophenyl)thio)-2,4,6-tris(*p*-tolylthio)-benzene(**3**–)).

Introduction

Because synthetic pathways to and structural and reactivity properties of biologically relevant iron–sulfur clusters with nuclearity of four or less have been demonstrated in considerable detail,¹ attention is increasingly directed toward the synthetic challenges of more complex protein-bound metal–sulfur clusters. Among them is a class of clusters designated as “bridged assemblies”, in which two or more recognizable fragments are juxtaposed wholly or in part by one or more covalent bridges.^{2,3} Among the well-known members of this class are the active site of sulfite reductase ([Fe₄S₄](μ_2 -S_{Cys})-[Fe(siroheme)]),^{4,5}

and the P-cluster ([Fe₄S₃](μ_2 -S_{Cys})₂(μ_6 -S)-[Fe₄S₃]) and FeMocofactor cluster ([Fe₄S₃](μ_2 -S)₃(μ_6 -X)-[MoFe₃S₃]) of nitrogenase.^{6–8} Recent protein crystallographic results have defined other members of this class found in carbon monoxide dehydrogenases. These enzymes catalyze the reversible reduction of carbon dioxide at the C-cluster site and, if bifunctional, the synthesis of acetyl coenzyme A from carbon monoxide, a methyl group, and coenzyme A at the A-cluster site.^{9,10}

The A-clusters of CODH¹¹ are minimally formulated as [Fe₄S₄](μ_2 -S_{Cys})-[M((μ_2 -S_{Cys})₂Gly)Ni]. Here, distal Ni^{II} is coordinated in a planar S₂N₂ environment of a deprotonated

[†] Harvard University.

[‡] Carnegie Mellon University.

- (1) Venkateswara Rao, P.; Holm, R. H. *Chem. Rev.* **2004**, *104*, 527–559.
- (2) Holm, R. H. *Pure Appl. Chem.* **1995**, *67*, 217–224.
- (3) Lee, S. C.; Holm, R. H. *Chem. Rev.* **2004**, *104*, 1135–1157.
- (4) Crane, B. R.; Siegel, L. M.; Getzoff, E. D. *Science* **1995**, *270*, 59–67.
- (5) Crane, B. R.; Siegel, L. M.; Getzoff, E. D. *Biochemistry* **1997**, *36*, 12120–12137.

- (6) Peters, J. W.; Stowell, M. H. B.; Soltis, S. M.; Finnegan, M. G.; Johnson, M. K.; Rees, D. C. *Biochemistry* **1997**, *36*, 1181–1187.
- (7) Mayer, S. M.; Lawson, D. M.; Gormal, C. A.; Roe, S. M.; Smith, B. E. *J. Mol. Biol.* **1999**, *292*, 871–891.
- (8) Einsle, O.; Tezcan, F. A.; Andrade, S.; Schmid, B.; Yoshida, M.; Howard, J. B.; Rees, D. C. *Science* **2002**, *297*, 1696–1700.
- (9) Ragsdale, S. W.; Kumar, M. *Chem. Rev.* **1996**, *96*, 2515–2539.
- (10) Grahame, D. A. *Trends Biochem. Sci.* **2003**, *28*, 221–224.

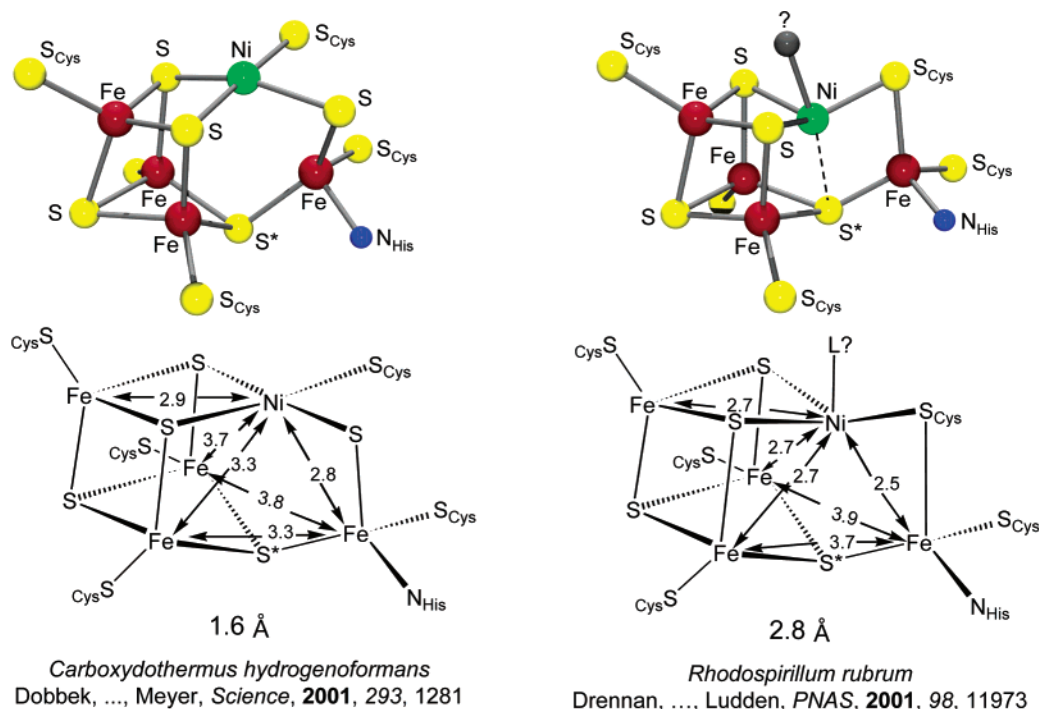


Figure 1. X-ray structures of the C-clusters of *C. hydrogenoformans* CODH at 1.6 Å resolution and *R. rubrum* at 2.8 Å resolution. Selected interatomic distances are indicated. A significant Ni–S* bonding interaction in the latter cluster is questionable.

Cys-Gly-Cys sequence and is bridged to a proximal metal $M = \text{Cu}^{\text{I}}$ (tetrahedral),¹² Zn^{II} (tetrahedral),¹³ and Ni^{II} (planar).¹³ These metal sites are coupled to an Fe_4S_4 cluster by a cysteinyl bridge. Current experimental evidence^{13,14} and computational results¹⁵ imply that nickel is the native metal. The formidably complicated C-clusters are structurally quite distinct from the A-clusters and are of pertinence in this work. Two clusters, one from *Carboxydotherrnus hydrogenoformans* CODH determined at 1.6 Å¹⁶ and the other from *Rhodospirillum rubrum* CODH obtained with 2.8 Å data,¹⁷ are described in Figure 1. The clusters qualify as bridged assemblies inasmuch as each has a tetrahedrally coordinated exo iron atom bridged to a larger fragment through two sulfur atoms, reported as two sulfides in one cluster and one sulfide and one cysteinyl in the other. The difference in bridging multiplicity of one of these sulfur atoms (S*) depends on its distance from the nickel atom. The separation in the *Ch* cluster is 3.8 Å, leading to planar four-coordinate nickel and a $\text{NiFe}_4(\mu_2\text{-S})(\mu_3\text{-S})_4$ core. The structure of the *Rr* cluster was originally presented as containing a cubane-like $\text{NiFe}_3(\mu_3\text{-S})_4$ fragment in a NiFe_4S_4 core.¹⁷ However, as observed by Drennan and co-workers,^{17,18} these incongruities

may arise from differences in resolution of the data and/or perhaps because they represent different chemical states of the same cluster.¹⁹

The closest synthetic approach to either CODH C-cluster structure is found in a set of NiFe_3S_4 cubane-type clusters prepared in this laboratory about 10 years before the advent of the protein structures. These clusters are obtained by two methods: (i) fragment condensation of the linear cluster $[\text{Fe}_3\text{S}_4(\text{SR})_4]^{3-}$ with a Ni^0 reactant followed by core rearrangement to the final cubane geometry;^{20,21} (ii) reaction of cuboidal $[\text{Fe}_3\text{S}_4(\text{LS}_3)]^{3-}$ with $[\text{Ni}^{\text{I}}(\text{PPh}_3)_3\text{Cl}]$, which affords the cubane cluster by fragment condensation.²² Both methods yield $[\text{NiFe}_3\text{S}_4]^{1+}$ clusters in which bonded Ni–S distances occur in the range 2.25–2.28 Å and the Ni^{II} site is tetrahedrally coordinated.^{20,21} These clusters, the C-clusters, and all other iron–sulfur clusters of physiological relevance (excepting the dinuclear fragment of the sites in [Fe]-hydrogenases) are weak field clusters, rendered so by the nature of the ligand sets.³ As such, they are characterized by (exchange-coupled) high-spin metal sites and the attendant kinetic lability of terminal ligands.

We note in the present context that certain bridged biological assemblies, their complicated structures notwithstanding, are yielding to chemical synthesis. It has been possible to synthesize a sulfide-bridged version of the sulfite reductase site²³ and to reproduce the topology of the nitrogenase P-cluster in the P^{N} state.^{24–28} In approaching the C-cluster structure, at least two

- (11) Abbreviations: bdt, benzene-1,2-dithiolate(2-); *Ch*, *Carboxydotherrnus hydrogenoformans*; dmpb, 1,2-bis(dimethylphosphino)benzene; CODH, carbon monoxide dehydrogenase; dmpe, 1,2-bis(dimethylphosphino)ethane; dppe, 1,2-bis(diphenylphosphino)ethane; Fd, ferredoxin; LS_3 , 1,3,5-tris-(4,6-dimethyl-3-mercaptophenyl)thio)-2,4,6-tris(*p*-tolylthio)benzene(3-); mes, mesityl; *Rr*, *Rhodospirillum rubrum*.
- (12) Doukov, T. I.; Iverson, T. M.; Seravalli, J.; Ragsdale, S. W.; Drennan, C. L. *Science* **2002**, 298, 567–572.
- (13) Darnault, C.; Volbeda, A.; Kim, E. J.; Legrand, P.; Vernède, X.; Lindahl, P. A.; Fontecilla-Camps, J. C. *Nat. Struct. Biol.* **2003**, 10, 271–279.
- (14) Bramlett, M. R.; Tan, X.; Lindahl, P. A. *J. Am. Chem. Soc.* **2003**, 125, 9316–9317.
- (15) Schenker, R. P.; Brunold, T. C. *J. Am. Chem. Soc.* **2003**, 125, 13962–13963.
- (16) Dobbek, H.; Svetlitchnyi, V.; Gremer, L.; Huber, R.; Meyer, O. *Science* **2001**, 293, 1281–1285.
- (17) Drennan, C. L.; Heo, J.; Sintchak, M. D.; Schreiter, E.; Ludden, P. W. *Proc. Natl. Acad. Sci. U.S.A.* **2001**, 98, 11973–11978.
- (18) Drennan, C. L.; Peters, J. W. *Curr. Opin. Struct. Biol.* **2003**, 13, 220–226.

- (19) The structure of the C-cluster of *M. thermoacetica* (f. *Clostridium thermoaceticum*) reveals a Ni–S* distance inconsistent with a significant bonding interaction: Drennan, C. L., private communication.
- (20) Ciurli, S.; Ross, P. K.; Scott, M. J.; Yu, S.-B.; Holm, R. H. *J. Am. Chem. Soc.* **1992**, 114, 5415–5423.
- (21) Zhou, J.; Scott, M. J.; Hu, Z.; Peng, G.; Münck, E.; Holm, R. H. *J. Am. Chem. Soc.* **1992**, 114, 10843–10854.
- (22) Zhou, J.; Raebiger, J. W.; Crawford, C. A.; Holm, R. H. *J. Am. Chem. Soc.* **1997**, 119, 6242–6250.
- (23) Zhou, C.; Cai, L.; Holm, R. H. *Inorg. Chem.* **1996**, 35, 2767–2772.
- (24) Zhang, Y.; Zuo, J.-L.; Zhou, H.-C.; Holm, R. H. *J. Am. Chem. Soc.* **2002**, 124, 14292–14293.

Table 1. Crystallographic Data for Two Solvated Forms of $(\text{Et}_4\text{N})_2[(\text{dmpe})\text{NiFe}_3\text{S}_4(\text{LS}_3)]^a$

	$(\text{Et}_4\text{N})_2[\mathbf{3a}]\cdot 2.5\text{MeCN}$	$(\text{Et}_4\text{N})_2[\mathbf{3b}]\cdot 0.25\text{MeCN}$
formula	$\text{C}_{156}\text{H}_{217}\text{Fe}_6\text{N}_9\text{Ni}_2\text{P}_4\text{S}_{26}$	$\text{C}_{147}\text{H}_{203.5}\text{Fe}_6\text{N}_{4.5}\text{Ni}_2\text{P}_4\text{S}_{26}$
<i>F</i> w	3628.44	3443.94
crystal system	triclinic	triclinic
space group	<i>P</i> 1	<i>P</i> 1
<i>Z</i>	2	2
<i>a</i> , Å	18.295(2)	18.219(4)
<i>b</i> , Å	18.925(2)	18.485(4)
<i>c</i> , Å	27.004(4)	27.031(5)
α , deg	78.940(4)	70.974(4)
β , deg	89.892(3)	83.543(5)
γ , deg	82.579(3)	79.737(5)
<i>V</i> , Å ³	9097(2)	8454(3)
<i>d</i> _{calc} , g·cm ⁻¹	1.328	1.346
μ , mm ⁻¹	1.048	1.122
θ , range, deg	1.22–25.00	1.43–23.00
GOF (<i>F</i> ²)	0.762	0.963
<i>R</i> ₁ , ^b <i>wR</i> ₂ ^c	0.047, 0.084	0.063, 0.127

^a Collected using Mo $K\alpha$ ($\lambda = 0.71073$ Å) radiation at $T = 193$ K. ^b $R_1 = \sum ||F_o| - |F_c|| / \sum |F_o|$. ^c $wR_2 = \{ \sum [w(F_o^2 - F_c^2)^2] / \sum [w(F_o^2)^2] \}^{1/2}$.

unprecedented steps are involved: creation of a planar Ni^{II} coordination unit within a NiFe_{3.4}S_{4.5} core, and stabilization of an exo iron atom bridged to the larger core fragment. This report deals with the former step.

Experimental Section

Preparation of Compounds. All operations were carried out under a pure dinitrogen atmosphere using standard glovebox or Schlenk techniques. Solvents were dried and degassed prior to use. The compound $(\text{Et}_4\text{N})_2[(\text{Ph}_3\text{P})\text{NiFe}_3\text{S}_4(\text{LS}_3)]$ (**2**) was prepared from the reaction of $(\text{Et}_4\text{N})_3[\text{Fe}_3\text{S}_4(\text{LS}_3)]^{29}$ (**1**) and $[\text{Ni}(\text{PPh}_3)_3\text{Cl}]$ as described elsewhere.²² The cluster salt was obtained as a mixture with 2 equiv of Ph₃P and 1 equiv of Et₄NCl. The mixture was used because of the stabilizing effect on the cluster in solution by excess phosphine.

$(\text{Et}_4\text{N})_2[(\text{dmpe})\text{NiFe}_3\text{S}_4(\text{LS}_3)]$ (**3**). To a solution of 30.1 mg of the cluster **2** mixture in 3 mL of acetonitrile was added a solution of 6.0 μL (36 μmol) of dmpe in 0.5 mL of acetonitrile. The solution was stirred for 1 h and was filtered. Vapor diffusion of ether into the filtrate afforded the pure product as 8.0 mg (ca. 45%) of black needles, which are highly dioxygen-sensitive. ¹H NMR (298 K, CD₃CN, anion): δ 1.53 (Me-dmpe), 2.29 (4'-Me), 5.19 (br, CH₂-dmpe); 6.39, 7.21 (3'-H, 2'-H); 13.53, 17.36 (4-Me, 6-Me); 18.20 (5-H). The yield was based on the cluster mixture $(\text{Et}_4\text{N})_2[\mathbf{2}]/2\text{Ph}_3\text{P}/\text{Et}_4\text{NCl}$. This preparation can be scaled up, but minor impurities are evident in the ¹H NMR spectra of the isolated solid. Multiple preparations on this scale proved the most satisfactory in obtaining a pure product. The compound was identified by an X-ray structure determination.

X-ray Structure Determinations. Vapor diffusion of ether into acetonitrile solutions of $(\text{Et}_4\text{N})_2[(\text{dmpe})\text{NiFe}_3\text{S}_4(\text{LS}_3)]$ resulted in the formation of the two solvated forms specified in Table 1. Both forms are triclinic and cannot be reliably distinguished by morphology. Their existence was verified by full structure determinations. Crystals were mounted in Infineum oil and placed in a dinitrogen cold stream on a Siemens (Bruker) SMART CCD-based diffractometer. Cell parameters were retrieved with SMART software and were refined using SAINT on all observed reflections. Data were collected in 0.3° intervals in φ and ω for 45 s/frame such that a hemisphere of data was collected. A total of 1271 frames was collected with a maximum resolution of 0.75 Å. The first 50 frames were re-collected at the end of the data collection

to monitor crystal decay; none was found. The highly redundant data sets were reduced using SAINT and corrected for Lorentz and polarization effects. Absorption corrections were applied using SHELX-97. The positions of metal atoms and their first coordination spheres were found in alternating difference Fourier syntheses and least-squares refinement cycles and, during the final cycles, were refined anisotropically. Hydrogen atoms were placed in calculated positions and refined as riding atoms with a uniform value of U_{iso} . Crystallographic parameters and agreement factors are contained in Table 1.³⁰

Sample Preparation. Samples containing cluster **3** were prepared in multiple batches as described above, yielding a total of 56 mg of black crystalline product. Crystals from each batch were withdrawn and examined by single-crystal X-ray diffraction. These were determined to be one of the two triclinic forms in Table 1; that is, the batches are physical mixtures of the two forms (clusters **3a** and **3b**). For ¹H NMR, Mössbauer, EPR, electrochemical, and mass spectrometric measurements, portions of these batches were employed. In EPR determinations, a 1.1 mM solution in glass-forming toluene/acetonitrile was used. Cluster **3** is extraordinarily sensitive to dioxygen and consequent decomposition and must be handled accordingly.

Other Physical Measurements. ¹H NMR spectra were obtained with a Bruker AM-400 spectrometer. Electrochemical measurements were carried out in acetonitrile solutions with a PAR model 263 potentiostat/galvanostat using a Pt working electrode and 0.1 M (Bu₄N)(ClO₄) supporting electrolyte. Potentials were measured at 298 K and are referenced to a SCE. Mössbauer spectra were recorded in two spectrometers that allowed measurements at temperatures between 1.5 and 240 K in parallel applied fields up to 8.0 T. Isomer shifts are quoted relative to iron metal at 298 K. The spectra were analyzed using the software WMOSS (WEB Research, Edina, MN). EPR spectra were recorded on a Bruker EPR 300 spectrometer equipped with an Oxford ESR 910 liquid helium cryostat and a Oxford temperature controller. The spectra were analyzed using a software package written by Prof. M. P. Hendrich of Carnegie Mellon University. Electrospray ionization mass spectra were recorded on a LCT mass spectrometer.

Results and Discussion

We seek synthetic pathways to the C-cluster of CODH as part of our research on the construction of bridged biological assemblies. Because of its higher resolution, we take the cluster of *Ch* CODH, with the core composition NiFe₄S₅, as the currently most accurate structural description of a C-cluster. Consequently, this cluster is the immediate object of synthesis. However, at this early stage of the problem, we note that its oxidation state and electronic features have not been reported, nor has it been established that the structure is that of a catalytically active cluster. The C-cluster of *Moorella thermoacetica* CODH has been the subject of extensive spectroscopic investigations;^{31,32} its three-dimensional structure is under investigation.¹⁹ Although the *Ch* CODH cluster structure in its entirety has no precedent, at least two fragments are familiar. The cuboidal Fe₃S₄ portion is found in numerous proteins and has been synthesized in the form of $[\text{Fe}_3\text{S}_4(\text{LS}_3)]^{3-}$.²⁹ Further, as noted, the cuboidal cluster will incorporate a nickel atom to form a cubane-type cluster similar in structure to that depicted for the C-cluster of *Rr* CODH. The planar NiS₄ unit is a conventional structural element in Ni^{II} complexes with both thiolate^{33,34} and metallasulfide^{35–37} ligands, an example of the

(25) Zhang, Y.; Holm, R. H. *J. Am. Chem. Soc.* **2003**, *125*, 3910–3920.
 (26) Zuo, J.-L.; Zhou, H.-C.; Holm, R. H. *Inorg. Chem.* **2003**, *42*, 4624–4631.
 (27) Ohki, Y.; Sunada, Y.; Honda, M.; Katsada, M.; Tatsumi, K. *J. Am. Chem. Soc.* **2003**, *125*, 4052–4053.
 (28) Zhang, Y.; Holm, R. H. *Inorg. Chem.* **2004**, *43*, 674–682.
 (29) Zhou, J.; Hu, Z.; Münck, E.; Holm, R. H. *J. Am. Chem. Soc.* **1996**, *118*, 1966–1980.

(30) See Supporting Information.
 (31) Hu, Z.; Spangler, N. J.; Anderson, M. E.; Xia, J.; Ludden, P. W.; Lindahl, P. A.; Münck, E. *J. Am. Chem. Soc.* **1996**, *118*, 830–845.
 (32) DeRose, V. J.; Telsler, J.; Anderson, M. E.; Lindahl, P. A.; Hoffman, B. M. *J. Am. Chem. Soc.* **1998**, *120*, 8767–8776.
 (33) Baidya, N.; Mascharak, P. K.; Stephan, D. W.; Campagna, C. F. *Inorg. Chim. Acta* **1990**, *177*, 233–238.

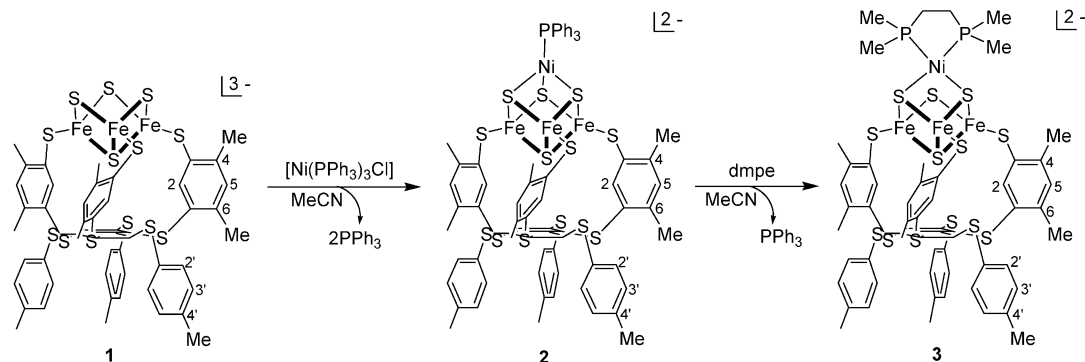


Figure 2. Synthesis of $[(\text{dmpe})\text{NiFe}_3\text{S}_4(\text{LS}_3)]^{2-}$ by introduction of a nickel atom into cuboidal cluster **1** to form the cubane-type cluster **2** followed by substitution of Ph_3P with dmpe to give **3** containing a planar $\text{Ni}^{\text{II}}\text{P}_2\text{S}_2$ coordination unit.

latter being $[\text{Ni}(\text{S}_2\text{Fe}_2(\text{CO})_6)_2]^{2-}$.³⁷ While tetrahedral Fe^{II} in a predominant or exclusive sulfur environment is entirely common, an exo-bridged arrangement whereby a single metal atom is covalently coupled to an iron–sulfur cluster is not. While there are several precedents of this general structure type,^{38–40} none involve sulfide bridges.

Cluster Synthesis. In this work, we address the problem of creating a planar diamagnetic Ni^{II} site in an iron–sulfur cluster. We have utilized a cubane-type NiFe_3S_4 cluster whose site-specific reactions with ligands sufficiently strong to induce Ni^{II} spin-pairing can potentially afford the desired structure. The first indications that this might be possible are found in reactions of $[(\text{Ph}_3\text{P})\text{NiFe}_3\text{S}_4(\text{SEt})_3]^{2-}$ ($S = 3/2$) with the chelating diphosphines dmpe and dmpb . Resonances attributed to $\text{Fe}-\text{SCH}_2$ groups occurred at $\delta \approx 120$ ppm, with isotropic shifts about twice as large as the parent cluster.²⁰ This result suggested a ground state with $S > 3/2$, because of the conversion of tetrahedral Ni^{II} to a diamagnetic site and removal of antiferromagnetic coupling between the $S = 1$ site and the $[\text{Fe}_3\text{S}_4]^{1-}$ fragment with probable spin $S = 5/2$.^{41,42} The observation was not pursued because of instability of the complexes and the attendant difficulty in crystallizing pure products. For the purpose at hand, we have turned to the cluster $[(\text{Ph}_3\text{P})\text{NiFe}_3\text{S}_4(\text{LS}_3)]^{2-}$,²² containing the semirigid cavitand-type ligand LS_3 which we have utilized in a number of reaction systems to promote site-specific reactivity and improve product stability.¹ Given the precedented planar diamagnetic $\text{cis-Ni}^{\text{II}}\text{P}_2\text{S}_2$ structures formed by 1,2-diphosphines and thiolate ligands,^{43–48} dmpe was selected as the strong-field ligand.

The successful reaction system is depicted in Figure 2. The cuboidal cluster $[\text{Fe}_3\text{S}_4(\text{LS}_3)]^{3-}$ (**1**) is converted to the cubane-

type cluster $[(\text{Ph}_3\text{P})\text{NiFe}_3\text{S}_4(\text{LS}_3)]^{2-}$ (**2**) by a fragment condensation reaction.³ Cluster **2** undergoes ligand substitution with dmpe to afford $[(\text{dmpe})\text{NiFe}_3\text{S}_4(\text{LS}_3)]^{2-}$ (**3**), which was obtained as a black air-sensitive crystalline solid in ca. 45% isolated yield. Clusters **2** and **3** are readily distinguished by their isotropically shifted ^1H NMR spectra (vide infra). Cluster **3** is characterized in its ES negative ion mass spectrum, shown in Figure 3, by a set of peaks centered at m/z 1449.1. The isotope distribution corresponds to the parent ion $[(\text{dmpe})\text{NiFe}_3\text{S}_4(\text{LS}_3)]^{1-}$ (M^{1-}). A second prominent peak occurs at m/z 666.0; it is attributed to $[\text{M}^{1-} - (\text{dmpe}) + \text{Cl}]^{2-}$, a result of the loss of neutral dmpe and addition of chloride from the source. The structure of **3** required proof by single-crystal X-ray diffraction.

Structure of $[(\text{dmpe})\text{NiFe}_3\text{S}_4(\text{LS}_3)]^{2-}$. When crystallized from acetonitrile by vapor diffusion with ether, $(\text{Et}_4\text{N})_2[\mathbf{3}]$ was obtained as the two acetonitrile solvates in Table 1. Crystalline mixtures were generally obtained; conditions were not established under which exclusive formation of one crystalline form occurred. The two forms, containing clusters **3a** and **3b**, crystallize in triclinic space group $P\bar{1}$ with similar dimensions and $Z = 4$. The asymmetric unit of each form includes two inequivalent clusters, **A** and **B**, each of which occurs as a racemic pair. The structure of one complete cluster of **3a** is given in Figure 4; selected bond distances and angles for the four inequivalent clusters are collected in Table 2 together with depictions of the cluster cores. Because of the very large number of parameters, tabulated data are restricted to core interatomic and terminal metal–ligand distances and a small number of angles involving mainly the nickel site. A detailed analysis of the structures of LS_3 cluster species, applied to the conformations of inequivalent clusters in the Ph_4P^+ salt of $[\text{Fe}_4\text{Se}_4(\text{LS}_3)\text{Cl}]^{2-}$, is available.⁴⁹ A less extensive description is given here.

All clusters crystallize in the *ababab* conformation with adjacent coordinating arms and buttressing *p*-tolylthio legs above (a) and below (b) the central phenyl ring. The cluster anions pack in a head-to-head and tail-to-tail style. The weak $\pi-\pi$ interactions between legs of the same and different clusters

- (34) Lim, B. S.; Fomitchov, D. V.; Holm, R. H. *Inorg. Chem.* **2001**, *40*, 4257–4262.
 (35) Sötofte, I. *Acta Chem. Scand. A* **1976**, *30*, 157–162.
 (36) Müller, A.; Bögge, H.; Krickemeyer, E.; Henkel, G.; Krebs, B. Z. *Naturforsch.* **1982**, *37b*, 1014–1019.
 (37) Holliday, R. L.; Roof, L. C.; Hargus, B.; Smith, D. M.; Wood, P. T.; Pennington, W. T.; Kolis, J. W. *Inorg. Chem.* **1995**, *34*, 4392–4401.
 (38) Wolff, T. E.; Berg, J. M.; Holm, R. H. *Inorg. Chem.* **1981**, *20*, 174–180.
 (39) Barrière, F.; Evans, D. J.; Hughes, D. L.; Ibrahim, S. K.; Talarmin, J.; Pickett, C. J. *J. Chem. Soc., Dalton Trans.* **1999**, 957–964.
 (40) Chen, C.; Wen, T.; Li, W.; Zhu, H.; Chen, Y.; Liu, Q.; Lu, J. *Inorg. Chem.* **1999**, *38*, 2375–2379.
 (41) Srivastava, K. K. P.; Surerus, K. K.; Conover, R. C.; Johnson, M. K.; Park, J.-B.; Adams, M. W. W.; Münck, E. *Inorg. Chem.* **1993**, *32*, 927–936.
 (42) Finnegan, M. G.; Conover, R. C.; Park, J.-B.; Zhou, Z. H.; Adams, M. W. W.; Johnson, M. K. *Inorg. Chem.* **1995**, *34*, 5358–5369.
 (43) Ramalingam, K.; Aravamudan, G.; Seshasayee, N.; Verghese, B. *Acta Crystallogr.* **1987**, *C43*, 471–473.
 (44) Akilan, R.; Sivakumar, K.; Venkatachalam, V.; Ramalingam, K.; Chinnakali, K.; Fun, H.-K. *Acta Crystallogr.* **1995**, *C51*, 368–370.

- (45) Tenorio, M. J.; Puerta, M. C.; Valerga, P. *J. Chem. Soc., Dalton Trans.* **1996**, 1935–1939.
 (46) Darkwa, J. *Inorg. Chim. Acta* **1997**, *257*, 137–141.
 (47) Hadjikostas, C. C.; Alkam, H. H.; Bolos, C. A.; Christidis, P. C. *Polyhedron* **2001**, *20*, 395–401.
 (48) Martins, M. A. C.; Silva, R. M.; Huffman, J. C. *Polyhedron* **2002**, *21*, 421–424.
 (49) Stack, T. D. P.; Weigel, J. A.; Holm, R. H. *Inorg. Chem.* **1990**, *29*, 3745–3760.

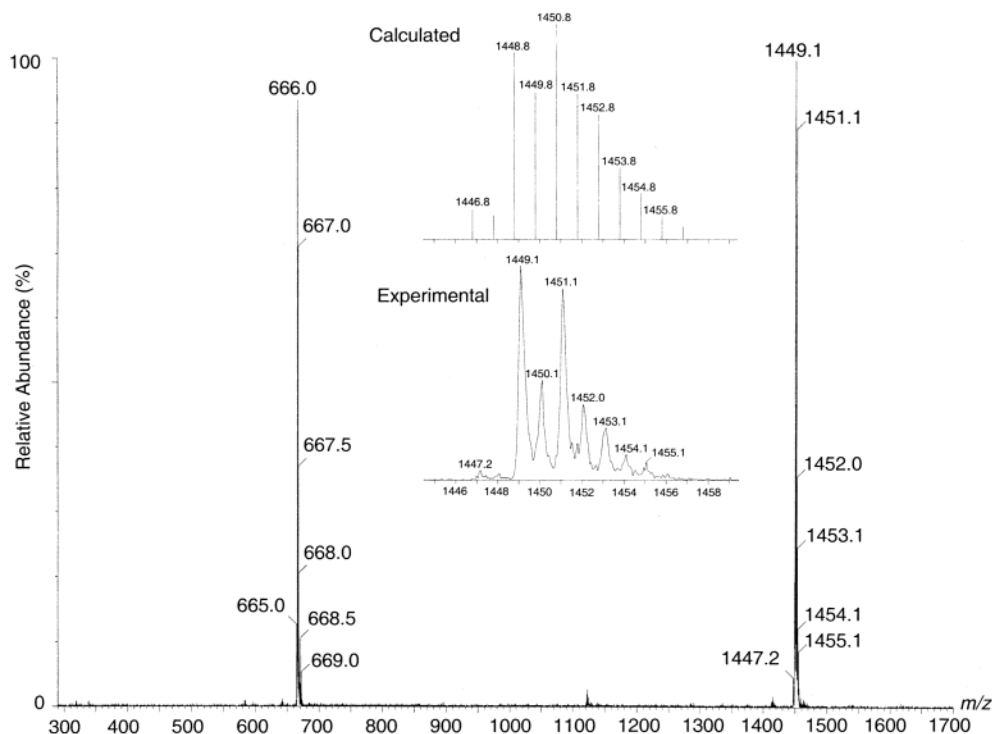


Figure 3. Electrospray negative ion mass spectrum of solvated $(\text{Et}_4\text{N})_2[\mathbf{3}]$. The insets are the calculated and experimental spectra of the set of peaks centered at m/z 1449.1 due to the parent ion $[(\text{dmpe})\text{NiFe}_3\text{S}_4(\text{LS}_3)]^-$.

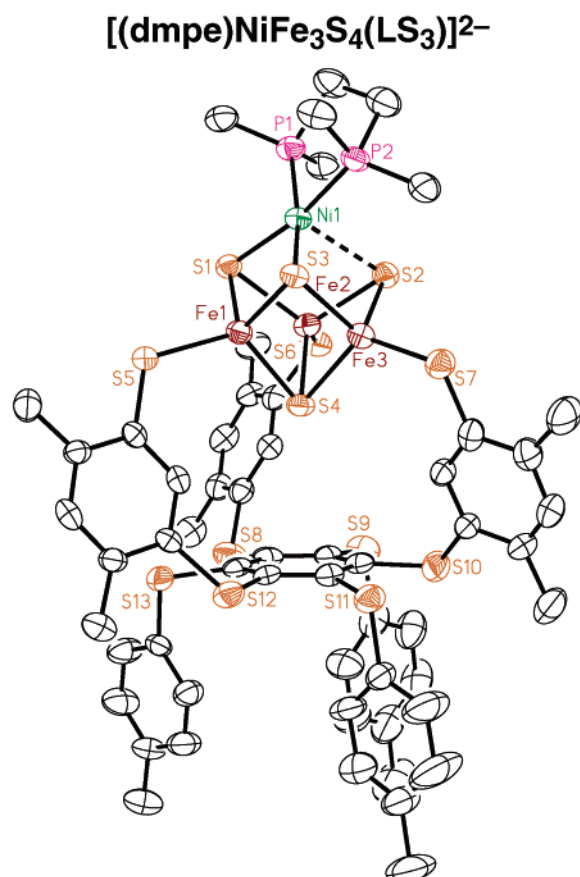


Figure 4. Structure of one of the two inequivalent clusters in the asymmetric unit of $(\text{Et}_4\text{N})_2[\mathbf{3a}] \cdot 2.5\text{MeCN}$, showing 50% probability ellipsoids and a partial atom labeling scheme.

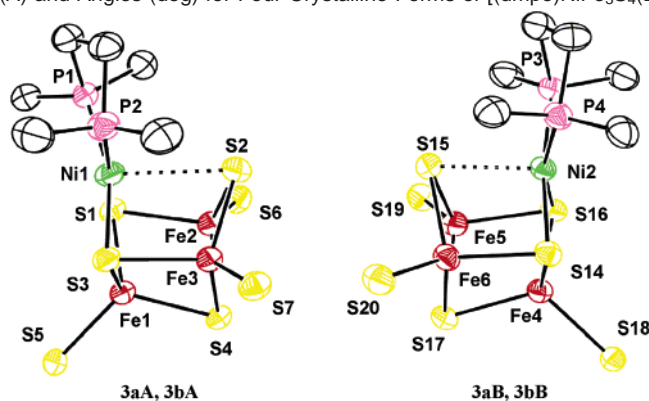
appear to influence the space available for solvate inclusion. The overall cluster stereochemistry is similar to Fe_4S_4 and

Fe_4Se_4 LS_3 species.^{49–51} Cluster **3** is the first structure of a heterometal core bound by LS_3 . The cluster core is coordinated at the three iron sites by sulfur atoms on ligand arms whose phenyl rings form dihedral angles of 43–86°. For example, in cluster **3aA**, the angles are 51.7°, 71.9°, and 85.5°. The cluster is positioned such that the distance between the centroid of the central ring and the closest core sulfide atom is 3.66–3.79 Å. In **3aA**, the S(4)–ring distance is 3.715 Å. The core structure deviates markedly from those of $[(\text{Ph}_3\text{P})\text{NiFe}_3\text{Se}_4(\text{SET})_3]^{2-}$ ²⁰ and $[(\text{Ph}_3\text{P})\text{NiFe}_3\text{S}_4(\text{Smes})_3]^{2-}$,²¹ in which the $\text{Ni}^{\text{II}}\text{PSe}_3$ and $\text{Ni}^{\text{II}}\text{PS}_3$ coordination units are *tetrahedral*. In cluster **3**, dmpe binds as a chelating ligand producing an $\text{Ni}^{\text{II}}\text{P}_2\text{S}_2$ unit that is essentially *planar*. The structures of all four clusters include this unit and are otherwise similar. As an example, we consider the structure of cluster **3aA**. Mean values given below refer to the four inequivalent clusters.

The least-squares plane fitted to the Ni(1)P(1,2)S(1,3) portion of **3aA** reveals a maximum deviation of 0.18 Å by the nickel atom; other deviations are ≤ 0.11 Å. Bond angles of cis ligand atoms range from 87.12(7)° for P1–Ni–P2 to 99.96(6)° for S1–Ni–S3. The former is a normal bite angle for a 1,2-diphosphine bound to planar Ni^{II} , as in, for example, $[\text{Ni}(\text{dppe})(\text{bdt})]$ (86.3°).⁴⁶ Trans P–Ni–S angles are 163.00(7)° and 170.37(7)°. The strong in-plane ligand field induced by coordination of dmpe results in the conspicuously long Ni1...S2 axial separation of 2.602(2) Å. In contrast, the bonded Ni(1)–S(1,3) distances average to 2.301 Å. In the two clusters with tetrahedral Ni^{II} sites, the mean Ni–S distances are somewhat shorter (2.262(2) and 2.273(9) Å). The Ni–P bond lengths of 2.149(2) and 2.150(2) Å are in the normal range of 2.14–2.17 Å for planar Ni^{II} . The Ni–S distances of 2.308(2) and 2.293(2) Å are notably long for anionic sulfur ligands bound to planar

(50) Stack, T. D. P.; Holm, R. H. *J. Am. Chem. Soc.* **1988**, *110*, 2484–2494.

(51) Zhou, C.; Holm, R. H. *Inorg. Chem.* **1997**, *36*, 4066–4077.

Table 2. Selected Bond Distances (Å) and Angles (deg) for Four Crystalline Forms of $[(\text{dmpe})\text{NiFe}_3\text{S}_4(\text{LS}_3)]^{2-}$ 

3aA		3aB		3bA		3bB	
Ni1–P1	2.149(2)	Ni2–P3	2.141(2)	Ni1–P1	2.161(3)	Ni2–P3	2.146(3)
Ni1–P2	2.150(2)	Ni2–P4	2.145(2)	Ni1–P2	2.132(3)	Ni2–P4	2.153(2)
Ni1–S1	2.308(2)	Ni2–S14	2.264(2)	Ni1–S1	2.255(2)	Ni2–S14	2.309(2)
Ni1–S3	2.293(2)	Ni2–S16	2.266(2)	Ni1–S3	2.319(2)	Ni2–S16	2.283(2)
Ni1–S2	2.602(2)	Ni2–S15	2.901(2)	Ni1–S2	2.748(3)	Ni2–S15	2.607(3)
Fe1–S1	2.299(2)	Fe4–S14	2.261(2)	Fe1–S1	2.294(3)	Fe4–S16	2.288(3)
Fe1–S3	2.274(2)	Fe4–S16	2.284(2)	Fe1–S3	2.285(3)	Fe4–S14	2.288(3)
Fe1–S4	2.303(2)	Fe4–S17	2.310(2)	Fe1–S4	2.314(2)	Fe4–S17	2.310(2)
Fe1–S5	2.331(2)	Fe4–S18	2.347(2)	Fe1–S5	2.294(2)	Fe4–S18	2.331(3)
Fe2–S1	2.329(2)	Fe5–S17	2.305(2)	Fe2–S1	2.312(3)	Fe5–S14	2.353(2)
Fe2–S2	2.262(2)	Fe5–S15	2.253(2)	Fe2–S2	2.269(3)	Fe5–S15	2.261(3)
Fe2–S4	2.321(2)	Fe5–S19	2.307(2)	Fe2–S4	2.322(3)	Fe5–S17	2.308(2)
Fe2–S6	2.317(2)	Fe5–S14	2.354(2)	Fe2–S6	2.312(3)	Fe5–S19	2.310(3)
Fe3–S2	2.263(2)	Fe6–S15	2.262(2)	Fe3–S2	2.275(2)	Fe6–S15	2.266(2)
Fe3–S3	2.357(2)	Fe6–S17	2.310(2)	Fe3–S3	2.339(2)	Fe6–S16	2.320(2)
Fe3–S4	2.303(2)	Fe6–S20	2.326(2)	Fe3–S4	2.323(3)	Fe6–S17	2.314(3)
Fe3–S7	2.311(2)	Fe6–S16	2.348(2)	Fe3–S7	2.315(3)	Fe6–S20	2.315(3)
Ni1–Fe1	2.904(1)	Ni2–Fe4	2.897(1)	Ni1–Fe3	3.195(2)	Ni2–Fe6	3.036(2)
Ni1–Fe2	3.031(1)	Ni2–Fe5	3.160(1)	Ni1–Fe2	2.980(2)	Ni2–Fe5	3.051(2)
Ni1–Fe3	3.046(1)	Ni2–Fe6	3.077(1)	Ni1–Fe1	2.928(2)	Ni2–Fe4	2.934(2)
Fe1–Fe2	2.726(1)	Fe4–Fe5	2.747(1)	Fe1–Fe2	2.772(2)	Fe4–Fe5	2.686(2)
Fe1–Fe3	2.728(1)	Fe4–Fe6	2.730(1)	Fe1–Fe3	2.764(2)	Fe4–Fe6	2.754(2)
Fe2–Fe3	2.717(1)	Fe5–Fe6	2.699(2)	Fe2–Fe3	2.694(2)	Fe5–Fe6	2.727(2)
Ni1–S4	4.236	Ni2–S17	4.290	Ni1–S4	4.259	Ni2–S17	4.256
S4–cent1 ^a	3.715	S17–cent2 ^a	3.665	S4–cent1 ^a	3.787	S17–cent2 ^a	3.758
P1–Ni1–P2	87.12(7)	P3–Ni2–P4	87.51(7)	P1–Ni1–P2	87.53(10)	P3–Ni2–P4	87.17(10)
P2–Ni1–S3	83.94(6)	P3–Ni2–S14	84.87(7)	P2–Ni1–S2	85.45(9)	P3–Ni2–S14	85.78(9)
P1–Ni1–S1	86.82(6)	P4–Ni2–S16	86.97(7)	P1–Ni1–S1	84.61(10)	P4–Ni2–S15	85.85(9)
S3–Ni1–S1	99.96(6)	S14–Ni2–S16	100.33(6)	S2–Ni1–S1	99.87(9)	S14–Ni2–S15	99.01(8)
P1–Ni1–S3	163.00(7)	P3–Ni2–S16	162.38(7)	P1–Ni1–S2	167.77(10)	P3–Ni2–S15	163.54(10)
P2–Ni1–S1	170.37(7)	P4–Ni2–S14	172.37(7)	P2–Ni1–S1	164.66(11)	P4–Ni2–S14	169.90(11)
Fe2–S2–Fe3	73.82(6)	Fe5–S15–Fe6	75.44(5)	Fe2–S2–Fe3	72.72(8)	Fe5–S15–Fe6	70.72(8)
Ni1–S1–S3/		Ni2–S15–S16/		Ni1–S1–S3/		Ni2–S15–S16/	
Fe1–S3–Fe3	162.9(2) ^b	Fe4–S15–S16	167.9(2) ^b	Fe1–S3–Fe3	169.5(3) ^b	Fe4–S15–S16	162.2(3) ^b
Fe2–S2–Fe3/		Fe5–S15–Fe6/		Fe2–S2–Fe3/		Fe5–S15–Fe6/	
Fe2–S4–Fe3	159.3(2) ^b	Fe5–S17–Fe6	154.1(2) ^b	Fe2–S4–Fe3	159.7(3) ^b	Fe5–S17–Fe6	157.9(3) ^b

^a Distance from S4 or S17 to the centroid of the middle phenyl ring. ^b Dihedral angle.

Ni^{II}, for which the usual range is 2.15–2.24 Å. The ranges quoted here are taken from a representative sampling of planar Ni^{II}P₂S₂ complexes and those with metallasulfido ligands.^{35–37,43–48} Consequently, the NiP₂S₂ unit in **3aA** and the other clusters is properly described in terms of slightly distorted square planar stereochemistry.

The most notable structure feature of each cluster is the long Ni⋯S core distance, which is variable across the set of clusters: **3aA**, 2.602(2) Å; **3aB**, 2.901(2) Å; **3bA**, 2.748 Å; **3bB**, 2.607(3) Å. The Ni₂Fe face and the Fe₂S₂ face opposite to it are nonplanar, as expressed by the appropriate dihedral angles (Table 2). The smallest dihedral angle in the Fe₂S₂ face, 154.1° in **3aB**, is associated with the longest Ni⋯S distance. Given the distances involved, it is evident that the sulfur atoms

(S15 in **3aB**) exert only weak axial interactions with the nickel atom. The atoms have the μ₂-S bridging modality with a mean Fe–(μ₂-S) bond length of 2.264(6) Å and Fe–S–Fe bridge angles of 70.7–75.4°. Within the core, the bond lengths follow the order Fe–(μ₃-S) > Fe–(μ₂-S), for which there are many examples^{25,52,53} and very few exceptions. Coordination of dmpe leads to a distorted square planar diamagnetic Ni^{II} coordination site similar to that in the *Ch* CODH cluster (Figure 1). The similarity extends to the nearly constant Ni–Fe distances in the Ni₂Fe face with a mean value of 2.92(2) Å, as compared

(52) Zhou, H.-C.; Su, W.; Achim, C.; Rao, P. V.; Holm, R. H. *Inorg. Chem.* **2002**, *41*, 3191–3201.

(53) Hagen, K. S.; Watson, A. D.; Holm, R. H. *J. Am. Chem. Soc.* **1983**, *105*, 3905–3913.

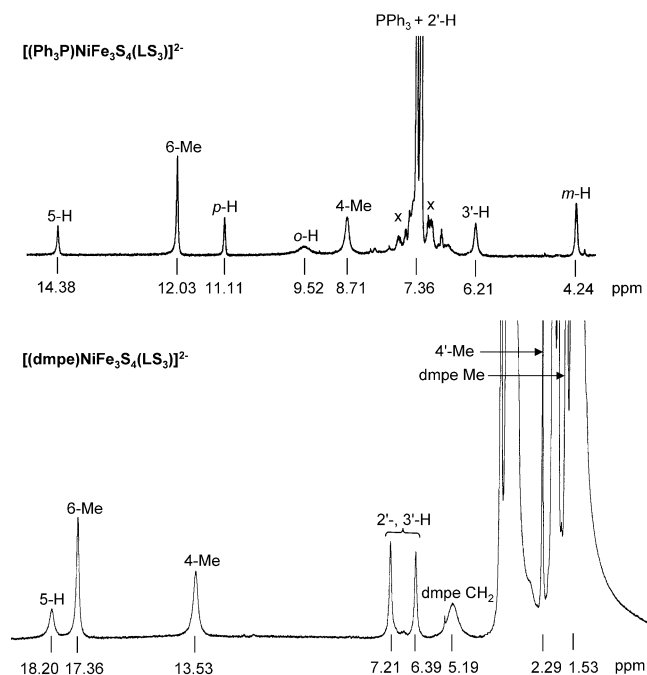


Figure 5. ^1H NMR spectra of clusters **2** (upper) and **3** (lower) in CD_3CN solutions at 298 K; chemical shifts are indicated.

to 2.9 Å in the protein cluster. Two other Ni–Fe separations (3.3, 3.7 Å) are longer than those in **3** (mean 3.07(7) Å), a consequence of the exo iron atom and the attendant Fe–(μ_3 -S)–Fe bridge.

A change in stereochemistry and spin state at a metal site induced by ligand substitution in weak-field cubane-type clusters, with retention of core composition, is preceded only by the reaction of isonitriles with $[\text{Fe}_4\text{S}_4]^{2+}$ clusters. Thus, treatment of $[\text{Fe}_4\text{S}_4(\text{LS}_3)\text{Cl}]^{2-}$ with excess RNC yields $[\text{Fe}_4\text{S}_4(\text{LS}_3)(\text{RNC})_3]^{1-}$, containing a six-coordinate low-spin Fe^{II} site and a $[\text{Fe}_3\text{S}_4]^0$ core fragment with $S = 2$.⁵⁴ Clusters containing two low-spin sites have been prepared from $[\text{Fe}_4\text{S}_4\text{Cl}_4]^{2-}$ and excess isonitrile.^{54,55}

Influence of Structure on Properties. The primary structural changes in the conversion of cluster **2** to cluster **3** are the introduction of the planar diamagnetic Ni^{II} site and the rupture of one Ni–(μ_3 -S) bond. This results in the formation of a magnetically isolated $\text{Fe}_3(\mu_2\text{-S})(\mu_3\text{-S})_3$ fragment similar in structure to the core of **1**, with the inverted bridging pattern $\text{Fe}_3(\mu_2\text{-S})_3(\mu_3\text{-S})$.

(a) ^1H NMR Spectra. The spectra of **2** and **3** are compared in Figure 5. The maximum idealized symmetry of **3** is C_3 , yet its spectrum reflects the trigonal symmetry appropriate to **2**. At temperatures down to 248 K in acetonitrile, the spectrum retains a single set of LS_3 resonances, indicating that **3** is fluxional. We suggest that the fluxional event is the making and breaking of Ni–S interactions with the result that two Ni–S bonds are permuted over the three sulfur atoms (S1, S2, S3 in Figure 4) nearest the nickel atom. (Note that reorientation of the dmpe chelate ring in a static NiFe_3S_4 core cannot average to trigonal symmetry.)

Other than the absence of Ph_3P resonances, the principal difference between the spectra at 298 K is that isotropic shifts

of 5-H, 4-Me, and 6-Me in **3** are 1.5–1.7 times larger than in **2**. Because isotropic shifts of ligands at the iron sites in Fe_3S_4 , Fe_4S_4 , and MFe_3S_4 clusters are well established to be mainly contact in origin and thus proportional to magnetic susceptibility,^{56,57} **3** is likely more paramagnetic than **2**. This situation could arise from different ground states or populations of ground and excited states. As will be seen, the ground states of the two clusters are different.

(b) Redox Series. In the cyclic voltammogram of cluster **3** in acetonitrile solution (100 mV/s, not shown), a chemically reversible step ($i_{\text{pa}}/i_{\text{pc}} \approx 1$) with $E_2 = -1.03$ V and an irreversible oxidation at $E_{\text{pa}} = -0.01$ V are observed. These results are placed in the context of the redox series of precursor Fe_3S_4 and other NiFe_3S_4 clusters in Table 3. The cores $[\text{Fe}_3\text{S}_4]^{2-}$ and $[\text{Ni}^{\text{II}}\text{Fe}_3\text{S}_4]^{2+}$ (isoelectronic except for Ni^{II}) are aligned vertically; spin states and redox potentials, where available, are included. In the three clusters with tetrahedral NiPS_3 sites, the Ni^{2+} charge may facilitate reduction to all-ferrous $[\text{NiFe}_3\text{S}_4]^0$. The $[\text{Fe}_3\text{S}_4]^{2-}$ state has been generated in proteins by proton-coupled electron transfer reactions.^{58,59} This oxidation state has not been achieved with **1**, probably because the 4– charge of the precursor cluster would shift the potential of the $[\text{Fe}_3\text{S}_4]^{1-/2-}$ couple to a very negative value. The $[\text{NiFe}_3\text{S}_4]^{1+/0}$ step was not detected with **3**. We conjecture that the $\text{Ni}(\text{dmpe})^{2+}$ fragment, more electron-rich than $\text{Ni}(\text{PPh}_3)^{2+}$, disfavors reduction to $[\text{NiFe}_3\text{S}_4]^0$ while affording an easier, reversible oxidation to $[\text{NiFe}_3\text{S}_4]^{2+}$ and a second oxidation which presumably reaches the unstable $[\text{NiFe}_3\text{S}_4]^{3+}$ state in an irreversible reaction. Of the various oxidation states in Table 3, only $[\text{Fe}_3\text{S}_4]^0$ and $[\text{NiFe}_3\text{S}_4]^{1+}$ in two structural configurations have thus far been isolated in the form of analogue clusters. The latter species has been obtained in protein-bound form where its $S = 3/2$ ground state,^{41,60} in common with that demonstrated for $[(\text{Ph}_3\text{P})\text{NiFe}_3\text{S}_4(\text{Smes})_3]^{2-}$ by spectroscopic and magnetic measurements,²¹ indicates that it has the cubane-type geometry with tetrahedral Ni^{II} .

(c) Ground-State Spin. The diamagnetism of the nickel site in the $[\text{NiFe}_3\text{S}_4]^{1+}$ core of **3** implied by its planar structure leaves the $[\text{Fe}_3\text{S}_4]^{1-}$ fragment, formally containing $2\text{Fe}^{\text{II}} + \text{Fe}^{\text{III}}$. This oxidation state has been observed for the protein-bound $[\text{ZnFe}_3\text{S}_4]^{1+}$ clusters in *Desulfovibrio gigas* Fd II⁶¹ and *Pyrococcus furiosus* Fd.^{41,42} by Mössbauer, EPR, and MCD spectroscopic studies. The consensus electronic description involves a valence-delocalized $\text{Fe}^{2.5+}\text{Fe}^{2.5+}$ pair with nearly equivalent iron sites and a high-spin $\text{Fe}^{\text{II}}\text{S}_4$ ($S = 2$) site. The valence delocalization is associated with double exchange within a formally $\text{Fe}^{3+}\text{Fe}^{2+}$ pair of sites. Belinsky⁶² has analyzed the ^{57}Fe magnetic hyperfine interactions of the $[\text{ZnFe}_3\text{S}_4]^{1+}$ protein-bound cluster and concluded that the $S = 5/2$ cluster ground state is a quantum mechanical mixture of four $S = 5/2$ configurations for which the delocalized pair has spin $S_{\text{pair}} = 9/2, 5/2, \text{ and } 3/2$, with a small contribution from $S_{\text{pair}} = 7/2$. The

(54) Weigel, J. A.; Srivastava, K. K. P.; Day, E. P.; Münck, E.; Holm, R. H. *J. Am. Chem. Soc.* **1990**, *112*, 8015–8023.

(55) Goh, C.; Weigel, J. A.; Holm, R. H. *Inorg. Chem.* **1994**, *33*, 4869–4877.

(56) Bertini, I.; Turano, P.; Vila, A. *J. Chem. Rev.* **1993**, *93*, 2833–2932.

(57) Bertini, I.; Ciurli, S.; Luchinat, C. *Struct. Bonding* **1995**, *83*, 1–53.

(58) Duff, J. L. C.; Breton, J. L. J.; Butt, J. N.; Armstrong, F. A.; Thomson, A. *J. Am. Chem. Soc.* **1996**, *118*, 8593–8603.

(59) Hirst, J.; Jameson, G. N. L.; Allen, J. W. A.; Armstrong, F. A. *J. Am. Chem. Soc.* **1998**, *120*, 11994–11999.

(60) Johnson, M. K.; Duderstadt, R. E.; Duin, E. C. *Adv. Inorg. Chem.* **1999**, *47*, 1–82.

(61) Surerus, K. K.; Münck, E.; Moura, I.; Moura, J. J. G.; LeGall, J. *J. Am. Chem. Soc.* **1987**, *109*, 3805–3807.

(62) Belinsky, M. I. *Chem. Phys.* **2001**, *263*, 279–300.

Table 3. Electron Transfer Series of Fe₃S₄ and NiFe₃S₄ Clusters

cluster		oxidation state ^a		ref		
[Fe ₃ S ₄] ²⁻	[Fe ₃ S ₄] ¹⁻	↔	[Fe ₃ S ₄] ⁰	↔	[Fe ₃ S ₄] ¹⁺	27
[Fe ₃ S ₄ (LS ₃) ³⁻	<i>S</i> = 5/2 ^b	-1.67 V ^c	<i>S</i> = 2	-0.79 V	<i>S</i> = 1/2 ^b	
[NiFe ₃ S ₄] ⁰	↔	[NiFe ₃ S ₄] ¹⁺	↔	[NiFe ₃ S ₄] ²⁺	[NiFe ₃ S ₄] ³⁺	this work
[(dmpe)NiFe ₃ S ₄ (LS ₃) ²⁻	-1.45 V	<i>S</i> = 3/2	-1.03 V	-0.01 V ^e		20
[(Ph ₃ P)NiFe ₃ S ₄ (LS ₃) ²⁻	-1.55 V	<i>S</i> = 3/2	-0.42 V ^e	-		19
[(Ph ₃ P)NiFe ₃ S ₄ (Smes) ₃] ^{2-f}	-1.62 V	<i>S</i> = 3/2	-0.50 V ^e	-		18
[(Ph ₃ P)NiFe ₃ S ₄ (SET) ₃] ²⁻			-0.58 V ^e	-		

^a States isolated in analogue clusters underlined. ^b Data for protein clusters. ^c Potentials in acetonitrile versus SCE. ^d Process not observed. ^e *E*_{pa} for irreversible process. ^f mes = mesityl.

Table 4. Comparison of Mössbauer Parameters of Cluster **3** and [ZnFe₃S₄]¹⁺ (*S* = 5/2)

	polycrystalline 3 ^a			[ZnFe ₃ S ₄] ¹⁺ ^{a,b}		
	1α	2α	2'α	1	2a	2b
<i>A</i> _z / <i>g</i> _n β _n (T)	5.0	-10.6	-	4.8	-	-
δ (mm/s) ^c	0.64	0.54	0.54	0.62	0.51	0.54
Δ <i>E</i> _Q (mm/s)	2.74	1.36	1.36	-2.7	+1.6	+1.6
η ^d	1.0	0	0	0.8	0.5	-2
α (deg) ^d	72	0	0	0	0	0
β (deg) ^d	20	48	31	30	33	15

^a Designation of sites: 1α, 1, Fe^{II}; 1α/2α, 2a/2b, delocalized pair. ^b Data for *D. gigas* Fd II; those for *P. furiosus* Fd are similar. ^c ±0.03 mm/s. ^d For **3**, the parameter set η_i, α_i, β_i is one set in an infinite manifold of parameters yielding the same spectrum at 1.5 K in weak applied fields (the so-called ambiguity problem).

calculated magnetic hyperfine tensors *A* are very sensitive to small variations of the (antisymmetric) exchange constants *J*, a point which we return to below. We seek to determine if a corresponding description applies to **3**. Mössbauer parameters and ⁵⁷Fe hyperfine data are given in Table 4. Note the close agreement between the isomer shifts of **3** and the protein cluster, signifying equivalent oxidation levels.

(1) Mössbauer Spectra. Measurements were performed on mixtures of solvated microcrystalline samples of (Et₄N)₂[**3**]. The spectra, shown in Figures 6 and 7, are exceedingly complex; we offer several comments to rationalize some of the complexity. First, the sample contains two solvated polycrystalline forms, (Et₄N)₂[**3a**] and (Et₄N)₂[**3b**]. As shown below, at least two spectroscopic forms, labeled **3α** and **3β**, are present, and, as the proportions of **3a** and **3b** are unknown, the various spectroscopic components must not occur in the same proportions. ESMS clearly reveals the presence of **3** as a parent ion and a credible fragmentation product formed by loss of dmpe and acquisition of chloride. The ¹H NMR spectrum (Figure 5) shows no evidence of another cluster species in the sample. Hence, **3α** and **3β** represent NiFe₃S₄ clusters. Second, ca. 10–15% of the iron in sample has become oxidized, which is not surprising given the redox potential of -1.03 V and the extreme sensitivity of the material to dioxygen. Third, the presence of at least six paramagnetic spectral components (each to be described with perhaps 10 unknown hyperfine parameters) with unknown zero-field splitting parameters, and the unknown oxidized components, yields spectra that presently can be described only qualitatively.

The Mössbauer spectrum shown in Figure 7 was recorded at 1.5 K in a magnetic field of 0.05 T applied parallel to the γ-rays. An identical spectrum was observed when the field was applied perpendicular to the γ-ray beam. This information together with the observation of a paramagnetic hyperfine structure in zero

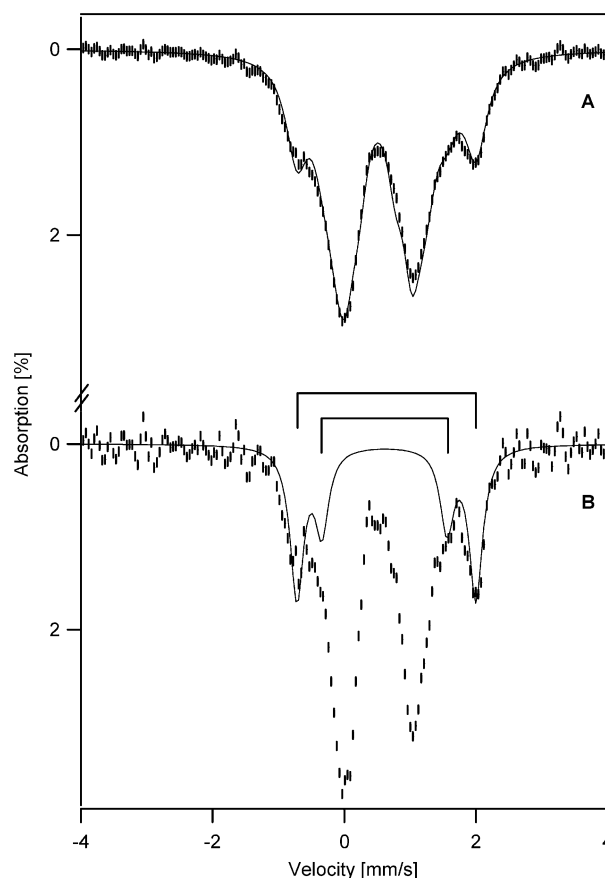


Figure 6. (A) Mössbauer spectrum of solvated polycrystalline (Et₄N)₂[**3**] at 77 K; the solid line is a spectral simulation using the parameters of Table 4. (B) Data of (A) after a resolution-enhancing Fourier transform procedure. Doublets 1α (more intense outer feature) and 1β are outlined by a spectral simulation. The central feature of spectrum (A) is represented by a superposition of four doublets, all with δ-values ranging from 0.5 to 0.56 mm/s; as the feature is not well-resolved, this representation is arbitrary.

field (not shown) implies that the electronic ground state of **3** is a Kramers doublet with effective *g*-values *g*_z ≫ *g*_x, *g*_y.⁶³ Such a doublet is generally EPR-silent, in accord with the data presented in Figure 8. We suggest below that the ground-state cluster spin is *S* = 5/2, at least for the majority component **3α**. At 4.2 K, some broader features appear, connoting that excited states of the ground-state spin multiplet become populated at this temperature. For this reason, we confine our analysis to the 1.5 K spectrum.

At temperatures above 50 K, the electron spin relaxation of **3** is fast on the Mössbauer time scale, as witnessed by the

(63) Münck, E. Aspects of ⁵⁷Fe Mössbauer Spectroscopy. In *Physical Methods in Inorganic and Bioinorganic Chemistry*; Que, L., Jr., Ed.; University Science Books: Sausalito, CA, 2000; Chapter 6.

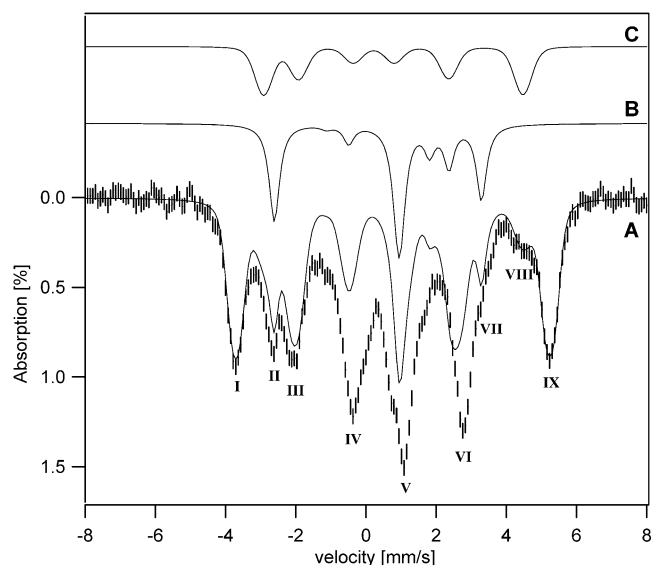


Figure 7. (A) Mössbauer spectrum of solvated polycrystalline $(\text{Et}_4\text{N})_2[3]$ at 1.5 K in a parallel field of 0.05 T. The Roman numerals label features discussed in the text. The solid line is a spectral simulation based on eq 1 for the three sites of 3α (54% of total iron) and site 2β (10%). Some of the absorption in IV and V reflects unknown oxidation products. Simulations for ferrous site 1α (B, 18%) and site 2β (C, 10%) are shown above the data.

observation of only quadrupole doublets. The spectrum of Figure 6A, recorded at 77 K, contains a doublet with quadrupole splitting $\Delta E_Q(1\alpha) = 2.72(4)$ mm/s and isomer shift $\delta(1\alpha) = 0.64(3)$ mm/s, parameters characteristic of a high-spin $\text{Fe}^{\text{II}}\text{S}_4$ site.⁶⁴ This site accounts for 21(2)% of total iron. A second $\text{Fe}^{\text{II}}\text{S}_4$ site with $\Delta E_Q(1\beta) = 1.90(5)$ mm/s and $\delta(1\beta) = 0.64(3)$ mm/s, accounting for ca. 10–12% of the iron, is revealed when the resolution is improved by subjecting the data to a Fourier transform (FT) procedure.⁶⁵ Doublets of the two Fe^{II} sites are indicated in the FT-treated spectrum of Figure 6B. The remainder of the absorption belongs to a broad doublet in the central part of the spectrum with $\delta_{\text{av}} \approx 0.54$ mm/s. For the simulation in Figure 6A, we have, quite arbitrarily, represented the central feature by four doublets with the $(\delta, \Delta E_Q)$ values (0.54, 1.36), (0.54, 0.97), (0.50, 1.04), and (0.50, 0.56) mm/s. Simulation of the central feature serves mainly as a reference to determine the fraction of iron represented by sites 1α and 1β . At temperatures above 77 K, the quadrupole splittings of the Fe^{II} sites are strongly temperature-dependent, and the doublets merge into the central feature with attendant loss of resolution.

The outermost lines in the 1.5 K spectrum of **3**, designated I and IX in Figure 7, are components of a six-line pattern characteristic of a magnetically anisotropic Kramers doublet, likely belonging to a valence-delocalized pair ($2\alpha/2'\alpha$) with $\delta = 0.54$ mm/s. Simulations could not generate line II as part of this pattern. Further, to produce a simulation with lines I, III, VI, and IX in the correct positions, the electric field gradient tensor of sites ($2\alpha, 2'\alpha$) must be rotated relative to the frame describing the zero-field splitting tensor. Thus, the symmetry

of the sites is less than rhombic. Studies in applied fields up to 7.0 T reveal that line II and shoulder VII move outward with increasing applied field; that is, the effective component of the magnetic hyperfine tensor, A_z , is positive. Other lines move inward with increasing field, implying sites with $A_z < 0$. Simulations suggest that lines II and VII belong to the Fe^{II} site with $\Delta E_Q = 2.72$ mm/s, that is, 1α . The calculated spectrum of this site is trace B in Figure 7. In the final calculations, slightly different parameters have been used for sites 2α and $2'\alpha$, primarily to account for the shapes of lines I and IX. For the theoretical spectrum in Figure 7A, that sites 1α , 2α , and $2'\alpha$ each account for 18% of the total iron suggests that they belong to one cluster, designated 3α .

We note briefly several other features of spectrum of Figure 7A. Shoulder VIII represents another iron environment (2β) from the $\delta \approx 0.54$ mm/s group. From the simulation of Figure 7C, it represents ca. 10% of total iron; high-field spectra show that this site has $A_z < 0$. If this component represents one iron site (2β) in a second NiFe_3S_4 cluster, it could be paired with the second ferrous component, $\Delta E_Q(1\beta) = 1.90(5)$ mm/s (10%), and an unassigned third component (3β) to assemble as second cluster, 3β , representing ca. 30% of total iron. (Most likely, the outermost lines of 3β are contained in lines II and VI.) In this interpretation, clusters 3α and 3β together constitute ca. 84% of total iron. It is also possible to assign site 2β to cluster 3α , trading it for site 2α or $2'\alpha$. We include this interpretation in the spectral analysis to recover, at least provisionally, a higher total iron content than that of 3α alone. However, the data in Table 4 are confined to the sites of cluster 3α . Last, we have good evidence that a fraction of the sample, representing perhaps 10–15% of total iron, is more oxidized than cluster 3β and contributes intensity to the center of the spectrum of Figure 7A.

The theoretical spectrum in Figure 7A was generated with the $S = 5/2$ spin Hamiltonian of eqs 1 and 2 in which the symbols have their usual meanings and the index i sums over the three sites ($1\alpha, 2\alpha, 2'\alpha$) of cluster **3**. As noted, the analysis is restricted to the 1.5 K spectrum

$$H = \mathbf{S} \cdot \mathbf{D} \cdot \mathbf{S} + \beta \mathbf{S} \cdot \mathbf{g} \cdot \mathbf{B} + \sum_{i=1}^3 \{ \mathbf{S} \cdot \mathbf{A}_i \cdot \mathbf{I}_i - g_n \beta_n \mathbf{B} \cdot \mathbf{I}_i + H_Q(i) \} \quad (1)$$

$$H_Q(i) = \frac{eQV_{i,z'z'}}{12} \left[3I_{i,z'}^2 - \frac{15}{4} + \eta_i (I_{i,x'}^2 - I_{i,y'}^2) \right] \quad (2)$$

recorded at 0.05 T. We have no evidence that any state other than the ground Kramers doublet is populated at 1.5 K. Thus, the spectra do not depend on the magnitude of the zero-field splitting parameter D ; however, D must be negative. Because the ground doublet is magnetically uniaxial and EPR-silent (see below), we take $E/D = 0$ to describe the spectra. This choice produces the spin expectation values $\langle S_x \rangle = \langle S_y \rangle = 0$ and $\langle S_z \rangle$

(64) Presently, we are not able to relate the clusters identified by Mössbauer spectroscopy to any of the structures characterized crystallographically. Therefore, we distinguish the spectroscopically suggested clusters by labels α and β , designating Fe cluster sites with Arabic numerals.

(65) Celia Dibar-Ure, M.; Flinn, P. A. In *Mössbauer Effect Methodology*; Gruverman, I. G., Ed.; Plenum Press: New York, 1971; Vol. 7.

(66) Prior to obtaining diffraction-quality crystals containing **3a** and **3b**, we obtained a crystalline form whose X-ray structure revealed the presence of one molecule each of $[(\text{dmpe})\text{NiFe}_3\text{S}_4(\text{LS}_3)]^{2-}$ and its oxidized form $[(\text{dmpe})\text{NiFe}_3\text{S}_4(\text{LS}_3)]^{1-}$ together with three cations in the asymmetric unit. For that material, the oxidized form contributed in zero field and at 4.2 K quadrupole doublets, as expected for a non-Kramers system. Comparison of the Mössbauer spectra of that form with those of the present sample showed that the spectrum of the 2- cluster was nearly the same in both crystals. Matching of the spectra for both samples revealed that the present sample must contain 10–15% of oxidized material, observed as quadrupole doublets. The oxidized fraction is not necessarily the 1- cluster.

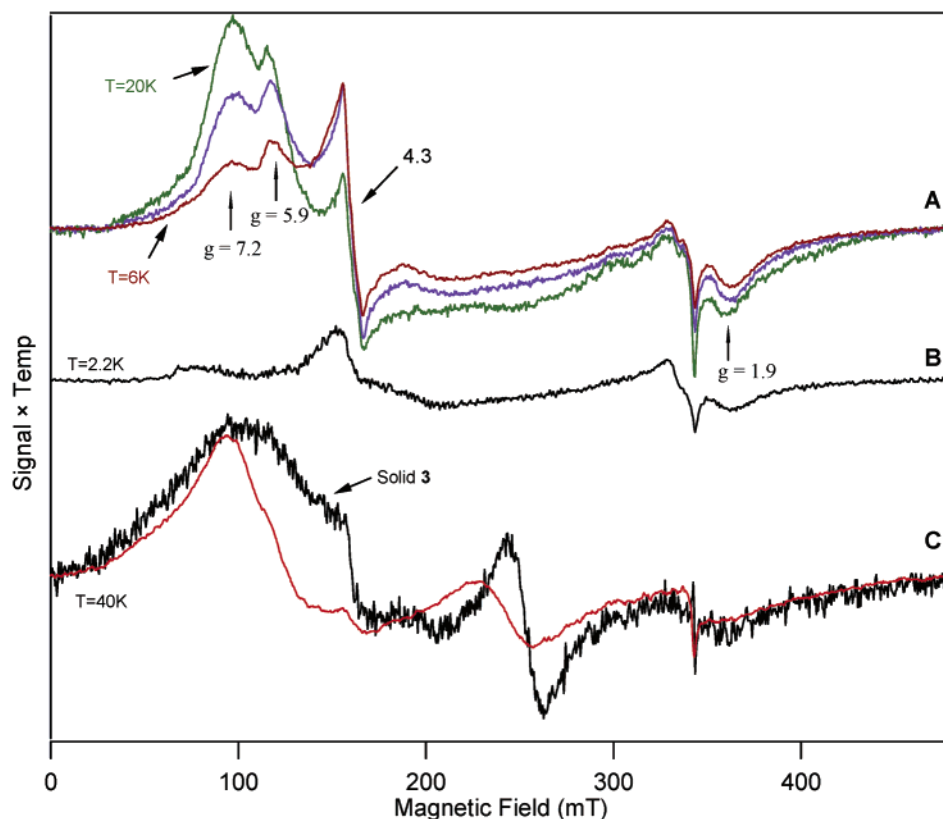


Figure 8. EPR spectra of solvated polycrystalline $(\text{Et}_4\text{N})_2[\mathbf{3}]$ and of ~ 1.1 mM $\mathbf{3}$ dissolved in toluene/acetonitrile (2:1 v/v). (A) Frozen solution spectra recorded at 2.2, 7, 11, and 20 K. For clarity, the 2.2 K spectrum has been offset as (B). Conditions: 9.62 GHz, 2 mW microwave power, 0.94 mT modulation. (C) Spectra at 40 K of solid $\mathbf{3}$ (noisy spectrum) and $\mathbf{3}$ in frozen solution at 0.2 and 20 mW microwave power, respectively. In these spectra, except for the $g = 1.9$ peak, the features near $g \approx 2$ are mainly cavity impurities.

$= \pm 5/2$. The internal magnetic field, B_{int} , determining the magnetic splittings is consequently fixed along the z -axis of the zero-field splitting tensor; $B_{\text{int}} = -\langle S_z \rangle A_z / g_n \beta_n$. Under these conditions, the Mössbauer spectra are described by specifying the direction of B_{int} by polar angles α_i, β_i in the principal axis frame (x', y', z') of the EFG tensor. It has been shown that under these conditions there exists a manifold of parameters α_i, β_i and asymmetry parameter η_i that produces the same Mössbauer spectra;⁶⁷ however, the magnitude of B_{int} is uniquely determined. Thus, the values given in Table 4 for α_i, β_i , and η_i are not unique.

In summary, the Mössbauer spectra of cluster $\mathbf{3}$ in the solid state reveal 10–15% oxidized material and at least two spectroscopically distinct $[\text{NiFe}_3\text{S}_4]^{1+}$ clusters. All evidence suggests that the Mössbauer sample was pure in the sense that the (two) $[\text{NiFe}_3\text{S}_4]^{1+}$ species observed here are likely representing one cluster that can exist in a physical mixture of states with distinct spectroscopic properties, rather than a sample containing $\mathbf{3}$ and some degradation product. We do not have a persuasive explanation for the presence of two cluster forms $\mathbf{3}\alpha$ and $\mathbf{3}\beta$. We have no evidence that $\mathbf{3}\alpha$ and $\mathbf{3}\beta$ have different cluster spins (see below). Perhaps, an explanation is suggested by the spin coupling model of Belinsky,⁶² who has shown that the A -tensors of the three sites of the $S = 5/2$ ground state of $[\text{ZnFe}_3\text{S}_4]^{1+}$ depend sensitively on the exchange coupling constants J_{ij} . In particular, for Belinsky's choice of parameters, the magnitudes of the A -tensors of the three sites drop

substantially when J_{13} is reduced from ~ 45 cm^{-1} to smaller values (see Figure 5b⁶²), and, moreover, the A -values of the pair become inequivalent. For $[\text{ZnFe}_3\text{S}_4]^{1+}$, the dependence of the J -values on the Fe–Fe distances is not known. Perhaps, minor metric changes in the cluster dimensions of $\mathbf{3}$ can substantially affect the magnetic properties of the $S = 5/2$ ground state, giving rise to the cluster state associated with Mössbauer component $\mathbf{3}\beta$.

(2) EPR Spectra. The presence of four distinct cluster forms in crystalline samples containing $\mathbf{3}$ undoubtedly reflects crystal packing effects. In the absence of ^{57}Fe -enriched material for solution Mössbauer studies, it was, therefore, of interest to examine $\mathbf{3}$ in suitable solvents by EPR. The X-band spectra of $(\text{Et}_4\text{N})_2[\mathbf{3}]$ in a toluene/acetonitrile glass are shown in Figure 8. At 2.2 K, we observed in all samples a broad feature at $g \approx 4$ possibly resulting from an $S = 3/2$ system with $E/D < 0.02$. This species is estimated from spectral simulations to account for only 4% of the total spin concentration. A second minor contaminant contributes a fairly intense derivative-shaped feature at $g = 4.3$ with considerable amplitude above 5 K, but the associated $S = 5/2$ system represents at best 2–3% of the spin concentration. Excited-state features, attributed to $\mathbf{3}$, are observed at $g = 7.2, 5.9$, and 1.9 ; the resonances at $g = 7.2$ and 5.9 are absent in the 2.2 K spectrum, consistent with the Mössbauer analysis. The 40 K spectra of Figure 8C compare polycrystalline and solution samples. The derivative features at $g = 2.7$ (solid) and 2.8 (solution) are presently not understood.

From a series of spectral simulations, we have concluded that the resonances at $g = 7.2$ and 5.9 most likely arise from one

(67) Dabrowski, L.; Piekoszewski, J.; Suwalski, J. *J. Nucl. Instrum. Methods* **1971**, *91*, 93–95.

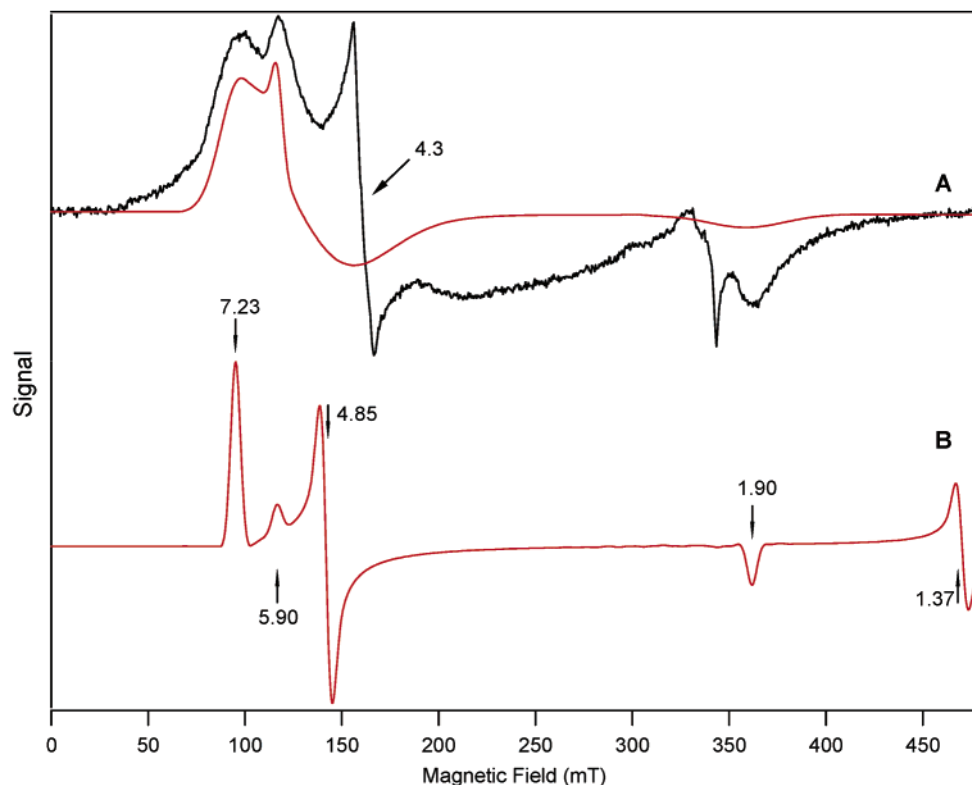


Figure 9. (A) EPR spectrum of **3** in toluene/acetonitrile at 11 K (same as Figure 8A). The smooth line is a spectral simulation for an $S = 5/2$ system with $D = -2 \text{ cm}^{-1}$, $E/D = 0.055$, and $g = 2.0, 2.0, 2.0$. To account for the low-field features (see text), we used $\sigma_{E/D} = 0.025$. (B) Spectral simulation for $\sigma_{E/D} = 0$, showing the resonances from the upper $M_S = \pm 1/2$ doublet at $g = 7.23, 4.85, 1.90$ and the $M_S = \pm 3/2$ doublet at $g = 5.90, 1.37$.

species⁶⁸ with $S = 5/2$, $D < 0$, and $E/D = 0.055$. For these parameters and an isotropic $g = 2.0$ in eq 1, the ground doublet $M_S = \pm 5/2$ has effective g -values at $g_x = g_y = 0$ and $g_z = 9.99$ and thus is EPR-silent. The first excited state, the $M_S = \pm 3/2$ doublet, has $g_x = 1.37$, $g_y = 1.24$, and $g_z = 5.90$, whereas for the upper $M_S = \pm 1/2$ doublet $g_x = 4.85$, $g_y = 7.23$, and $g_z = 1.90$. The trace in Figure 9B is a simulation of the 11 K spectrum for $D = -2 \text{ cm}^{-1}$ and $E/D = 0.055$. The features marked with the downward arrows designate the resonances of the $M_S = \pm 1/2$ doublet. The peak at $g = 5.90$ and the derivative feature at $g = 1.37$ belong to the middle doublet. For some complexes with $S > 1/2$, reasonable simulations of broad spectra have been obtained by assuming a Gaussian distribution of E/D with width $\sigma_{E/D}$. Inspection of plots of effective g -values of the three doublets versus E/D shows that some resonances such as the $g_x = 4.85$ and $g_x = 1.37$ features are drastically broadened by distributing E/D while others, such as that with $g_z = 5.90$, experience considerably less broadening. The smooth solid line in Figure 9A is a simulation using the same parameters as in Figure 9B but with $\sigma_{E/D} = 0.025$ instead of $\sigma_{E/D} = 0$. In this simulation, the low-field region shows the $g_y = 7.23$ and $g_z = 5.90$ peaks, while the broad trough at $g \approx 4.5$ belongs to the broadened $g_x = 4.85$ feature of the $M_S = \pm 1/2$ doublet. At 11 K, the $g_z = 5.90$ resonance, riding on the $g_y = 4.85$ derivative feature, has the largest amplitude. However, at higher temperature, the increasing population of the $M_S = \pm 1/2$ doublet, coupled with its intrinsically larger transition EPR probabilities,

causes the $g_y = 7.23$ resonance to become the most intense feature, as observed experimentally. We have not been able to subtract the $g = 4.3$ contaminant by finding a suitable spectral representation of its line shape, and thus we were not able to test our simulation in this critical region. Finally, the simulation of Figure 9A yields a $g = 1.90$ resonance that is too broad; this is not surprising given the simple line broadening model. Because the simulation does not match the experimental line shape sufficiently well, we hesitate to quote a value for D ; roughly, the magnitude of D is between 1.5 and 2.5 cm^{-1} , in good agreement with the D -values reported for $[\text{ZnFe}_3\text{S}_4]^{1+}$ clusters of *D. gigas* ferredoxin II ($D = -2.7 \text{ cm}^{-1}$)⁶¹ and *P. furiosus* ferredoxin ($D = -2.7, -2.5 \text{ cm}^{-1}$)^{41,42}. Interestingly, our simulations yield for $D = -2 \text{ cm}^{-1}$ a spin concentration of ca. 0.9 mM which is a significant fraction of the cluster concentration of the sample, $\sim 1.1 \text{ mM}$.

Summary

The following are the principal results and conclusions of this investigation:

(1) The tetrahedral Ni^{II} site in the cubane-type cluster $[(\text{Ph}_3\text{P})\text{NiFe}_3\text{S}_4(\text{LS}_3)]^{2-}$ can be converted to a planar diamagnetic configuration by reaction with a suitably strong-field ligand, here dmpe. This is the second example of stereochemical and spin state alteration in an iron–sulfur cluster by reaction with a strong-field ligand.

(2) In the reaction of **2** with dmpe, the initial axial ligand is lost, one $\text{Ni}-(\mu_3\text{-S})$ bond is broken, and the $[\text{Fe}_3(\mu_2\text{-S})(\mu_3\text{-S})_3]^{1-}$ and distorted square planar $\text{Ni}^{\text{II}}(\mu_3\text{-S})_2\text{P}_2$ ($\text{Ni}-\text{S}$ 2.26–2.32 Å, $\text{Ni}-\text{P}$ 2.13–2.16 Å, $\text{P}-\text{Ni}-\text{P}$ 87.1–87.5°, $\text{S}-\text{Ni}-\text{S}$ 99.0–

(68) Inversion of the relative intensities of the $g = 7.2$ and 5.9 resonances with increasing temperature raised the possibility that they belong to different species. Given that the Mössbauer spectra indicate multiple species, the assumption would not be unreasonable.

100.3°) fragments are created. In solvated $(\text{Et}_4\text{N})_2[(\text{dmpe})\text{-NiFe}_3\text{S}_4(\text{LS}_3)]$, four *edge-cleaved cubane* clusters are present which differ in their weak $\text{Ni}\cdots\text{S}$ axial interactions ranging from 2.60 to 2.90 Å. Of the known iron–sulfur clusters, $[\text{Fe}_3\text{S}_4]^{1-}$ is most closely related to $[\text{Fe}_3(\mu_2\text{-S})_3(\mu_3\text{-S})]^{0,1+}$ in analogue clusters and proteins.^{29,60}

(3) The major Mössbauer component present in solvated polycrystalline $(\text{Et}_4\text{N})_2[(\text{dmpe})\text{NiFe}_3\text{S}_4(\text{LS}_3)]$ appears to be a cluster (**3 α**) exhibiting ^{57}Fe hyperfine interactions quite similar to those reported for $[\text{ZnFe}_3\text{S}_4]^{1+}$ (Table 4) and accounting for ca. 54% of the iron in the sample. The similarity of the Mössbauer spectra of **3 α** with those of $[\text{ZnFe}_3\text{S}_4]^{1+}$ as well as our (tentative) interpretation of the EPR spectra of **3** suggests a cluster spin $S = 5/2$. A spectroscopically detected second cluster

(69) The second (tentatively identified) cluster type (**3 β**) exhibits parameters that differ substantially from those associated with **3 α** . Thus, the ΔE_Q -value of the Fe^{II} site (1.90 mm/s) is substantially smaller than that associated with the Fe^{II} site of **3 α** . Moreover, while the spectra of **3 α** suggest the presence of a delocalized $\text{Fe}^{2.5+}\text{Fe}^{2.5+}$ pair, such a pair does not seem to be present in **3 β** (10% of total Fe represents one iron site). If, on the other hand, spectral component **2 β** would represent a delocalized pair, the third (ferrous) site would have to represent ca. 5% of the iron in the sample. Because component **1 β** , however, accounts for about 10–12% of the iron, we prefer the interpretation that **2 β** represents a single iron atom. The presence of at least two cluster forms distinguishable by Mössbauer spectroscopy strongly suggests that there should also be at least two spectral forms (perhaps both with $S = 5/2$) in the EPR spectra of solid $(\text{Et}_4\text{N})_2[(\text{dmpe})\text{NiFe}_3\text{S}_4(\text{LS}_3)]$. Finally, it is not obvious how to relate the Mössbauer components seen in the polycrystalline samples with any of the four structures of cluster **3**.

(**3 β**) has not been fully identified.⁶⁹ The complexity of the Mössbauer spectrum is presumably due in part to the existence of different $[\text{NiFe}_3\text{S}_4]^{1+}$ cluster forms in the solvated polycrystalline solid examined.

(4) Isoelectronic cubane-type ($S = 3/2$) and edge-cleaved cubane ($S = 5/2$) clusters have different ground states, arising from the antiferromagnetic coupling of tetrahedral Ni^{2+} ($S = 1$) with $[\text{Fe}_3\text{S}_4]^{1-}$ ($S = 5/2$) or from the latter fragment alone, respectively. This accounts for the substantial difference in isotropically shifted ^1H NMR spectra.

(5) The formation of $[(\text{dmpe})\text{NiFe}_3\text{S}_4(\text{LS}_3)]^{2-}$ with its edge-cleaved cubane core offers a proof in principle that a planar site such as that in *Ch* CODH (Figure 1) can be created in a Ni–Fe–S cluster. It is the first step in constructing an $\text{NiFe}_4(\mu_2\text{-S})(\mu_3\text{-S})_4$ cluster with the attributes of physiological ligation at the planar Ni^{II} site and an exo iron atom coupled to an edge-cleaved cubane.

Acknowledgment. This research was supported by NIH Grant 28856 at Harvard University and NSF Grant MCD-9416624 at Carnegie Mellon University. We thank Dr. S. C. Lee for experimental assistance and useful discussion.

Supporting Information Available: X-ray crystallographic files for the compounds in Table 1. This material is available free of charge via the Internet at <http://pubs.acs.org>.

JA030627S